Short-term consolidation of articular cartilage in the long-term context of osteoarthritis

Woodhouse, F., Gardiner, B., & Smith, D. (2015). Short-term consolidation of articular cartilage in the long-term context of osteoarthritis. Journal of Theoretical Biology, 368, 102-112. DOI: 10.1016/j.jtbi.2015.01.003

Published in:
Journal of Theoretical Biology

DOI:
10.1016/j.jtbi.2015.01.003

Document Version
Peer reviewed version

Short-term consolidation of articular cartilage in the long-term context of osteoarthritis

Francis G. Woodhouse*, Bruce S. Gardiner, David W. Smith

Faculty of Engineering, Computing and Mathematics, The University of Western Australia, Perth, WA, Australia

Abstract

Over ten percent of the population are afflicted by osteoarthritis, a chronic disease of diarthrodial joints such as the knees and hips, costing hundreds of billions of dollars every year. In this condition, the thin layers of articular cartilage on the bones degrade and weaken over years, causing pain, stiffness and eventual immobility. The biggest controllable risk factor is long-term mechanical overloading of the cartilage, but the disparity in time scales makes this process a challenge to model: loading events can take place every second, whereas degradation occurs over many months. Therefore, a suitable model must be sufficiently simple to permit evaluation over long periods of variable loading, yet must deliver results sufficiently accurate to be of clinical use, conditions unmet by existing models. To address this gap, we construct a two-component poroelastic model endowed with a new flow restricting boundary condition, which better represents the joint space environment compared to the typical free-flow condition. Under both static and cyclic loading, we explore the rate of gradual consolidation of the medium. In the static case, we analytically characterise the duration of consolidation, which governs the duration of effective fluid-assisted lubrication. In the oscillatory case, we identify a region of persistent strain oscillations in otherwise consolidated tissue, and derive estimates of its depth and magnitude. Finally, we link the two cases through the concept of an equivalent static stress, and discuss how our results help explain the inexorable cartilage degeneration of osteoarthritis.

Keywords: tissue, biomechanics, aggrecan, collagen, poroelasticity

PACS: 46.70.-p, 47.56.+r, 87.10.Ed, 87.18.Nq, 87.19.R-, 87.19.xn, 87.85.-d

1. Introduction

As we walk and run around, our knees and hips endure forces many times our body weight. They withstand these megapascal-scale pressures (Hodge et al., 1986) thanks to a 1–4 mm thick coating of articular cartilage on the ends of the bones in these synovial joints (Hunziker et al., 2002). This coating performs two vital roles: it allows the opposing bones to slide smoothly against one another, and it protects the underlying bone from injurious stress concentrations (Bader et al., 2011).

The construction of articular cartilage is remarkably simple (Hunziker et al., 2002; Kiani et al., 2002), as illustrated in fig. 1. A solid matrix of collagen fibres entraps a high density of giant (∼200 MDa) bottlebrush-shaped aggregates of aggrecan molecules. Each aggrecan is itself also a large bottlebrush structure of mass 1–3.5 MDa (Bathe et al., 2005), comprising many charged glycosaminoglycans attached to a protein core. The charge density induces a high osmotic pressure, which swells the cartilage with water from the surrounding synovial fluid to form the tissue interstitial fluid (Tepic et al., 1983). Interspersed throughout the tissue are millions of chondrocyte cells, the only

*Corresponding author. E-mail: francis.woodhouse@uwa.edu.au

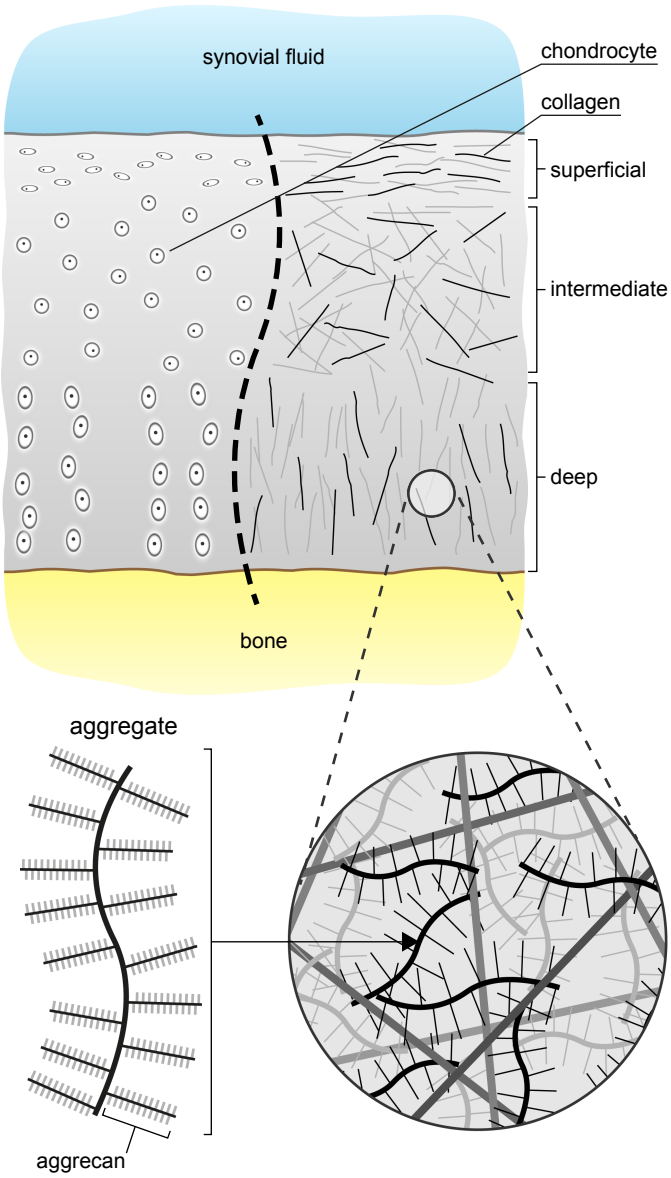

Figure 1: The construction of articular cartilage. Chondrocyte cells are interspersed throughout a solid matrix of collagen, which retains a dense suspension of giant bottlebrush-like aggregates of aggrecan molecules, themselves each a bottlebrush. The structure of the chondrocytes and collagen divides the non-calcified cartilage above the bone into the three distinct zones shown.

live components of articular cartilage, which synthesise all of the aggrecan and collagen (Goldring and Marcu, 2009).

Articular cartilage functions through its mechanical properties as a *poroelastic medium*: a porous elastic solid saturated with fluid. At the instant of loading, the interstitial fluid bears all of the stress. Driven by the pressure difference between the tissue and the synovial space in the joint, water gradually exudes through the cartilage surface into the synovial fluid, where it helps to lubricate sliding of opposing cartilage faces in so-called *mixed mode lubrication* (Ateshian, 2009; Gleghorn and Bonassar, 2008; Katta et al., 2008; McCutchen, 1962). As fluid is lost, the solid structure progressively deforms, transferring the load to elastic compression of the high-density aggregates. Finally, when the load is released, the cartilage re-imbibes fluid and swells.

If the loading is sufficiently frequent, the cartilage does not have time to re-swell to its original size each cycle. Instead, it undergoes *consolidation*: it will progressively compress by a greater fraction every time it is loaded, exuding less fluid and therefore contributing less to lubrication, until a state of maximal average compression and minimal average exudation is reached. As well as affecting the elastic modulus, the high density of aggregates also results in a low permeability of the solid to the interstitial fluid, yielding a functional consolidation time of an hour or more (Ateshian, 2009; Comper, 1991). During this time, the coefficient of friction rises ten-fold (Gleghorn and Bonassar, 2008).

In healthy tissue, chondrocytes synthesise new material to repair any damage caused by high levels of compression and friction in late-stage consolidation. However, if damage overtakes repair for some reason, the tissue gradually degrades over months or years. This debilitating condition, termed *osteoarthritis* (OA) or *non-inflammatory arthritis*, has a morbidity of over 10% of the population and costs the economy hundreds of billions of dollars every year in lost productivity (Bitton, 2009). Repairing the tissue is difficult (Hunziker, 2002; Newman, 1998), and in serious cases the only effective treatment may be surgical joint replacement.

The aetiology of OA is complex. Both genetic and behavioural risk factors exist. Of the latter, abnormal joint loading is particularly prominent. For instance, surgical alteration of the menisci—tough rings of fibrocartilage in

the knee which spread load over the articular cartilage—often causes early onset OA (Papalia et al., 2011), as does damage to ligaments, and certain occupations have higher rates of OA (Coggon et al., 2000). In these scenarios, the abnormal mechanical loading induces chondrocyte apoptosis and damages the solid matrix (Chen et al., 2001; Grodzinsky et al., 2000; Jones et al., 2009; Kurz et al., 2005; Sandell and Aigner, 2001). A vicious cycle begins: the depleted chondrocyte population cannot fully repair the solid matrix, so subsequent loading of the structurally compromised tissue causes more damage and apoptosis, leading to further inadequate repair, and so-on (Goggs et al., 2003). The onset of early-stage OA is therefore intimately linked with the mechanical response of the cartilage as a function of its integrity and loading patterns.

To quantify this response, we need a mechanical model. Early linear 'biphasic' models codified the process of consolidation (Ateshian et al., 1997), and complex finite element studies are developing this further (Haemer et al., 2012; Mononen et al., 2012; Pierce et al., 2013). Such studies predict large spatial variations of strain and pressure (Suh et al., 1995; Wong and Carter, 2003) and exhibit frequency dependent consolidation rates under cyclic loading (Suh et al., 1995; Zhang et al., 2014). However, these models are either prohibitively complex for use over the long time scales of OA development, or lack pertinent *in vivo* details. In particular, many studies use a free flow condition for the pore fluid efflux when, in reality, the close proximity of other tissues will restrict flow (Wong and Carter, 2003), potentially causing a marked slowdown in the long-term consolidation rate (Halonen et al., 2014).

In this paper we derive a simple, effective and tractable cartilage mechanics model explicitly from aggrecan and pore fluid dynamics. To model the effect of the narrow joint geometry *in vivo*, we introduce a new *flow restriction* boundary condition. We then study the model numerically and analytically, first under static and then oscillatory loading. In both cases, we characterise the dependence on loading and flow restriction of two key properties: the time taken to consolidate, which corresponds to the duration of mixed mode lubrication, and the strains experienced through the cartilage.

In the static case, we first illustrate the essential features of consolidation before exploring the influence of flow restriction. We show that greater restriction slows down consolidation, helping to preserve cartilage integrity. We derive an approximate relationship between the consolidation time scale, the applied load and the tissue's biomechanical properties, and demonstrate its robustness over a wide range of flow resistance values.

We then examine oscillatory loading, the more common usage pattern. First, we show that low levels of flow restriction at the surface markedly temper long-term variability in the total cartilage thickness compared to a free-flowing boundary, but significant strain variability persists in the superficial zone. To quantify this, we solve the consolidation problem linearised about the time-averaged strain field, which yields approximations for three primary quantities: the depth d of the high-strain region, the strain variation range Δ, and the propagation speed v of compression waves. We show that these quantities scale with the loading frequency f as $d \sim f^{-1/2}$, $\Delta \sim f^{-1/2}$ and $v \sim f^{1/2}$, and that Δ varies inversely with the boundary flow resistance.

The approximations we derive encapsulate the salient points of cartilage biomechanics. Our results quantify intuition as to why the early stages of OA depend so much on behavioural factors: if flow restriction is altered through surgery, or stresses are raised through abnormal posture or gait, then mixed mode lubrication time falls, strains and strain variability rise, and a potentially unrecoverable cycle of damage begins.

2. Cartilage model

Healthy, non-calcified articular cartilage is not homogeneous. As illustrated in fig. 1, it is typically divided

into three distinct regions (Changoor et al., 2011; Hunziker et al., 2002; Jadin et al., 2005). The outermost *superficial zone*, exposed to the synovial fluid within the joint capsule, makes up the first 5–10% of the thickness. It is characterised by surface-parallel collagen fibres and pancake-shaped chondrocytes. The next 15–20% is the *transitional* or *intermediate zone*, with isotropically-oriented fibres and scattered spherical chondrocytes. The remaining 70–80% comprises the *radial* or *deep zone*, wherein the matrix is oriented perpendicular to the bone and egg-shaped chondrocytes are arranged in regimented columns. We will often refer back to these zones, especially the exposed superficial zone.

Importantly, the aggrecan density is also inhomogeneous: the density in the superficial zone is half of that in the deep zone (Klein et al., 2007; Maroudas, 1976; Smith et al., 2013; Wedig et al., 2005). This implies that the superficial zone will experience greater strains and consolidate faster than if the distribution were homogeneous, while the opposite holds in the deep zone (Carter and Wong, 2003; Chen et al., 2001; Schinagl et al., 1996; Wilson et al., 2007). With this in mind, we now construct our cartilage biomechanics model.

2.1. Poroelastic equations

The geometry we will model is equivalent to a so-called 'confined compression' test. In such a test, a cylinder of cartilage is placed in a frictionless, impermeable well, tightly bounding all but its upper surface. A uniform, porous plate covers the exposed surface, through which the desired load is applied. The subsequent tissue compression is then measured over time. Due to the confinement, no lateral strain develops and flow through the tissue will only be vertical, with fluid exiting through the porous plate. Therefore, this geometry guarantees a one-dimensional deformation state, with purely vertical pressure gradient and strain profile.

Of course, the true *in vivo* cartilage loading scenario is not one-dimensional. However, it is a reasonable approximation in the more realistic case we consider here, where a thin planar cartilage 'slab' is bounded below by an impermeable bone interface and subjected to upper surface loading whose lateral extent is large relative to the tissue thickness. As well as simplifying specification and analysis of our model, this geometry allows us to extract the primary tissue behaviours without resorting to extensive numerical simulations.

We adopt a poroelastic (Biot, 1955; Verruijt, 1995) or 'biphasic' (Ateshian et al., 1997) model of cartilage, consisting of a particulate solid phase (representing the aggrecan, collagen, and other such constituents) saturated by fluid. Both solid and fluid phases are assumed to be intrinsically incompressible, so deformation is the result of fluid efflux and consequent elastic strain by mass conservation. In addition, as the strain in loaded cartilage can surpass 30% (Carter and Wong, 2003), a finite deformation model is necessary; in one dimension, specifying such a model is immensely simplified compared to higher dimensions.

The cartilage has unloaded thickness H, with comoving (material) coordinate z running from $z = 0$ at the bone to $z = H$ at the surface. We will couch our model in terms of the engineering strain ε, where $\varepsilon < 0$ in compression, with associated axial deformation gradient $F = 1 + \varepsilon$. The true cartilage thickness at time t is then

$$h(t) = \int_0^H F\,dz = H + \int_0^H \varepsilon\,dz.$$

The corresponding work conjugate to the deformation gradient is the first Piola–Kirchoff stress, but in one dimension its axial component coincides with that of the Cauchy stress; therefore, for consistency with the cartilage literature, we take the liberty of denoting axial stresses by σ, with $\sigma < 0$ in compression.

The total vertical stress σ_{tot} decomposes as $\sigma_{\mathrm{tot}} = -p(z,t) + \sigma(z,t)$, with fluid pressure $p(z,t)$ and solid stress $\sigma(z,t)$ (Verruijt, 1995). The solid stress $\sigma(z,t)$ in turn

depends on the strain $\varepsilon(z,t)$. At time t, the tissue is subject to a prescribed compressive vertical surface stress $\Sigma(t) \leqslant 0$ at $z = H$. Provided inertial and body forces are negligible, instantaneous equilibrium implies σ_{tot} satisfies $\partial\sigma_{\text{tot}}/\partial z = 0$, so it follows that $\sigma_{\text{tot}} = \Sigma(t)$ for all z. Given the relationship between solid stress σ and strain ε, as well as the time-dependent behaviour of the fluid pressure p as a function of ε, this equilibrium governs the behaviour of the tissue over time for a given loading profile $\Sigma(t)$.

We first define the solid stress σ. In compression, the collagen matrix contributes little strength, with most resistance supplied by the aggrecan (Han et al., 2011). Therefore, we neglect the contribution of collagen to the stress. Now, suppose that the unloaded cartilage possesses an aggrecan concentration distribution

$$c_0(z) = A_0 + (A_2 - A_0)(z/H)^2,$$

with $c_0(0) = A_0 > A_2 = c_0(H)$. This profile is typical of those observed in experiments (Wedig et al., 2005). At non-zero strain, the one-dimensional deformed volume element is $1+\varepsilon$, so the true aggrecan density in a compressed unit volume reads

$$c(z,t) = \frac{c_0(z)}{1+\varepsilon(z,t)}.$$

(In higher dimensions, this would read $c_0/\det(\mathbf{F})$, with $\mathbf{F}$ the deformation gradient tensor.) The high charge density of the aggrecan molecules induces a strong, non-ideal osmotic pressure Π which can be fitted with a virial expansion (Bathe et al., 2005; Comper, 1991)

$$\Pi(z,t) = RT\left[\alpha_1 c(z,t) + \alpha_2 c(z,t)^2 + \alpha_3 c(z,t)^3\right],$$

where R is the gas constant, T is the temperature, and the α_i are the virial expansion coefficients. It is this osmotic pressure which gradually supports a greater proportion of the load as the tissue strain develops towards steady state.

Absent loading, the osmotic pressure causes cartilage to swell. Ordinarily this swelling is restrained by the collagen network. Our neglect of the collagen here means we cannot simply write $\sigma = -\Pi$, but instead must augment the solid stress to mimic this restraint. We match $\varepsilon = 0$ to the unloaded swollen state and define an effective solid stress

$$\sigma(z,t) = \Pi_0(z)e^{\Lambda\varepsilon(z,t)} - \Pi(z,t), \tag{1}$$

where Π_0 is Π at $\varepsilon = 0$ (i.e. with $c = c_0$) and Λ is a large positive constant to model unloading and buckling of the collagen network under compression. This gives $\sigma = 0$ at $\varepsilon = 0$, and $\sigma \approx -\Pi$ for moderate compression ($\varepsilon < 0$). In fact, eq. (1) constitutes the stress in a hyperelastic material with local strain energy density function

$$W(\varepsilon) = RT\Bigg[(\alpha_1 c_0 + \alpha_2 c_0^2 + \alpha_3 c_0^3)\frac{e^{\Lambda\varepsilon}}{\Lambda} - \alpha_1 c_0 \log(1+\varepsilon) + \frac{\alpha_2 c_0^2}{1+\varepsilon} + \frac{\alpha_3 c_0^3}{2(1+\varepsilon)^2}\Bigg].$$

Note that a three-dimensional formulation of the stress would need to be in terms of appropriate work conjugates, such as the first Piola–Kirchoff stress tensor if using the deformation gradient as the strain measure as we do here. In addition, the planar tensile effects of collagen may need to be considered if the loading is sufficiently non-uniform, such as in an indentation test.

We now define the fluid pressure p. The interstitial flow obeys Darcy's law for flow in a porous medium (Batchelor, 2000), whereby the flux q is proportional to the gradient in pressure. In our Lagrangian viewpoint, this becomes

$$q(z,t) = -\frac{k(z,t)}{1+\varepsilon(z,t)}\frac{\partial p(z,t)}{\partial z}. \tag{2}$$

The function $k(z,t)$ is known as the permeability. The factor $1/(1+\varepsilon)$ serves to perform an inverse Piola transformation of the Eulerian permeability k into the Lagrangian frame, resulting in an effective Lagrangian permeability $K = k/(1+\varepsilon)$. This is derived in the appendix.

Denser aggrecan is less permeable, so k, like Π, is a function of the compressed aggrecan concentration c. The permeability fits a power law

$$k(z,t) = \frac{k_0}{c(z,t)^{\beta_k}},$$

where k_0 and β_k are positive constants (Comper and Lyons, 1993; Smith et al., 2013). An exponential relationship is a common alternative (Mow et al., 1984).

In reality, the permeability of the tissue to water is a function not only of the aggrecan density, but also of the collagen matrix geometry. As mentioned earlier, the collagen matrix varies in its orientation and density through the tissue depth (Muir et al., 1970; Nieminen et al., 2001), thus potentially adding a depth-dependent component to the basic permeability k_0. For clarity we neglect such effects here, since collagen density variation affects permeability rather less than aggrecan (Muir et al., 1970), but we note that a change in the volume fraction of water and aggrecan can be interpreted as a change in k_0.

Putting together Darcy's law and conservation of mass leads to the non-linear diffusion-type equation

$$\frac{\partial \varepsilon}{\partial t} = \frac{\partial}{\partial z}\left(\frac{k}{1+\varepsilon}\frac{\partial p}{\partial z}\right). \tag{3}$$

This is derived in the appendix, following Gibson et al. (1967, 1981) and McNabb (1960).

Combining eq. (3) with the equilibrium stress–strain relation

$$\Sigma = \sigma_{\text{tot}} = -p + \sigma = -p + \Pi_0 e^{\Lambda\varepsilon} - \Pi \tag{4}$$

yields a closed system. All that remains is to supply boundary conditions and the loading protocol for $\Sigma(t)$.

2.2. Boundary conditions

We take the bone boundary $z = 0$ to be impermeable, so $q(0,t) = 0$, which implies $p_z(0,t) = 0$ through eq. (2) (where p_z denotes $\partial p/\partial z$).

The condition at $z = H$ demands more careful consideration. A typical approach in consolidation problems is to suppose free flow through the upper surface by setting $p(H,t) = 0$ (Mow et al., 1984). In reality, the joint geometry will provide resistance to fluid exiting the cartilage surface. In the knee, for example, flow is restricted by the meniscus, as it forces the fluid to flow around and through its dense porous structure (Haemer et al., 2012). A simple way to model this is to write the pressure as proportional to the flux, essentially coupling the cartilage to another porous medium whose far end is held at zero reference pressure (in the synovial fluid). We write $p(H,t) = \gamma q(H,t)$, which implies the Robin-type condition

$$p(H,t) = \sigma(H,t) - \Sigma(t) = -\gamma\frac{k(H,t)}{1+\varepsilon(H,t)}p_z(H,t) \tag{5}$$

by eqs. (2) and (4). The proportionality constant $\gamma > 0$ dictates the resistance, with higher γ giving lower flux.

2.3. Loading protocol

We will consider both static and oscillatory loading, and reiterate that loads will always be compressive, so $\Sigma \leqslant 0$. Modelling static loading, where Σ is constant, serves two functions: to understand the reaction of cartilage to loading in vulnerable situations such as prolonged standing or kneeling, and to compare an oscillatory load profile with its equivalent mean static stress.

For oscillatory loading, we will mimic typical activity patterns using half-sinusoidal loading of frequency f and mean $\bar{\Sigma} \leqslant 0$. The instantaneous load is then

$$\Sigma(t) = \begin{cases} \bar{\Sigma}\pi\sin(2\pi f t) & \text{if } ft - \lfloor ft \rfloor \in [0, \frac{1}{2}], \\ 0 & \text{if } ft - \lfloor ft \rfloor \in [\frac{1}{2}, 1], \end{cases} \tag{6}$$

where $\lfloor\cdot\rfloor$ is the integer floor function, so $x - \lfloor x \rfloor$ is the fractional part of x. We will often compare oscillatory loading with the case of static loading under the same mean stress, where $\Sigma(t) \equiv \bar{\Sigma}$.

2.4. Non-dimensionalisation and parameter selection

We now non-dimensionalise the system in order to understand its parameter dependencies.

There are several natural scalings. First, let $z = H\hat{z}$, so the cartilage runs from $\hat{z} = 0$ to $\hat{z} = 1$. Now let $c = A_0\hat{c}$ and $c_0 = A_0\hat{c}_0$, so $\hat{c} = \hat{c}_0/(1+\varepsilon)$, yielding the rescaled aggrecan profile $\hat{c}_0(\hat{z}) = 1-(1-\phi)\hat{z}^2$ with $\phi = A_2/A_0$. This then suggests setting $k = k_0 A_0^{-\beta_k}\hat{k}$ to obtain $\hat{k} = \hat{c}^{-\beta_k}$.

Next, define the pressure scale $S = RT\alpha_1 A_0$. Let $\Pi = S\hat{\Pi}$, where $\hat{\Pi} = \hat{c} + a_2\hat{c}^2 + a_3\hat{c}^3$ with rescaled virial coefficients $a_2 = A_0\alpha_2/\alpha_1$ and $a_3 = A_0^2\alpha_3/\alpha_1$. This scaling for Π implies identical scalings for the fluid pressure $p = S\hat{p}$, total stress $\sigma_{\text{tot}} = S\hat{\sigma}_{\text{tot}}$ and applied load $\Sigma = S\hat{\Sigma}$.

Combining these parameter groups yields a time scale

$$\tau = \frac{A_0^{\beta_k - 1} H^2}{RT\alpha_1 k_0}.$$

Setting $t = \tau\hat{t}$ recasts eq. (3) into the dimensionless form

$$\frac{\partial\varepsilon}{\partial\hat{t}} = \frac{\partial}{\partial\hat{z}}\left(\frac{\hat{k}}{1+\varepsilon}\frac{\partial\hat{p}}{\partial\hat{z}}\right).$$

The cyclic loading frequency also then rescales as $f = \hat{f}/\tau$.

Finally, the boundary condition in eq. (5) rescales to

$$\hat{p}(1,\hat{t}) = -\Gamma\frac{\hat{k}(1,\hat{t})}{1+\varepsilon(1,\hat{t})}\hat{p}_{\hat{z}}(1,\hat{t}), \tag{7}$$

with rescaled boundary resistance

$$\Gamma = \frac{k_0 A_0^{-\beta_k}}{H}\gamma.$$

The form of τ implies a quadratic dependence of consolidation time on cartilage thickness H. This holds exactly for homogeneous, unrestricted consolidation (Verruijt, 1995). Here, however, the boundary resistance Γ goes inversely with H, and a lesser resistance promotes faster efflux, so the true effect on consolidation time of increasing H is likely sub-quadratic.

The original eleven parameters have been reduced to six: a_2, a_3, ϕ, β_k, Λ and Γ. Of these, we will fix the first five, as they correspond to material properties of the cartilage itself, whereas Γ, our new resistance parameter, is primarily related to the environment external to the cartilage. The values of the fixed physical parameters used, and the derived non-dimensional constants, are given in table 1. We have chosen parameters representative of typical healthy cartilage in order to demonstrate and explore this model numerically, but the values appropriate to different applications will vary with species, age, joint quality and tissue location (Korhonen et al., 2002; Shepherd and Seedhom, 1999). A realistic range of Γ is difficult to determine, since it depends heavily on the tissue environment *in vivo* and therefore cannot be determined by standard explant compression tests. In this work, we will explore values between $\Gamma = 0$ (free-flowing) and $\Gamma = 1$, later focussing on $\Gamma = 0.1$ as a value that has a noticeable but not unrealistically excessive effect.

Parameter	Value	
RT	$2.5\,\text{kPa mL}/\mu\text{mol}$ ($T \approx 300\,\text{K}$)	
α_1	$1.4 \times 10^{-1}\,\mu\text{mol/mg}$	⋆
α_2	$4.4 \times 10^{-3}\,\mu\text{mol mL/mg}^2$	⋆
α_3	$5.7 \times 10^{-5}\,\mu\text{mol mL}^2/\text{mg}^3$	⋆
k_0	$1.0 \times 10^{-3}\,\text{mm}^2(\text{mg/mL})^{\beta_k}/\text{kPa/s}$	†
β_k	1.6	†
A_0	$100\,\text{mg/ml}$	‡
A_2	$60\,\text{mg/ml}$	‡
Λ	30	
a_2	3.1	
a_3	4.1	
ϕ	0.6	

Table 1: Parameter values chosen. Derived non-dimensional values are below the line. ⋆ Bathe et al. (2005); † Comper and Lyons (1993) and Smith et al. (2013); ‡ Wedig et al. (2005).

The parameters in table 1 imply a pressure scale $S = 35\,\text{kPa}$, and here we will consider average loads up to $15S \approx 500\,\text{kPa}$. For a typical thickness $H = 3\,\text{mm}$ we also get a time scale $\tau = 4.1 \times 10^5\,\text{s}$, or 5 days; however, the majority of the consolidation process occurs in a small fraction of this time. Typical consolidation durations examined will be on the order of $\hat{t} = 0.01$, which is equivalent to approximately 1 hour with the above value of τ.

Having completed our rescaling, we now drop the hat notation where applicable and work exclusively with the non-dimensional variables unless otherwise specified.

3. Static loading

To illustrate the process of consolidation and to explore the fundamental effect of the boundary resistance, we begin by studying consolidation under a static stress.

The basic progression of consolidation is the following. At the instant of first loading, the stress is borne entirely through hydrostatic pressure of the pore fluid and the tissue is infinitely stiff. This creates a pressure gradient at the semi-permeable surface, which induces fluid efflux. As the pore fluid is exuded, the solid structure deforms, progressively transferring more of the load from hydrostatic pressure into elastic strain. Eventually an equilibrium is approached whereby the entire load is sustained by the solid phase and the remaining pore fluid is once again at background pressure ($p = 0$ here). This process is exemplified in fig. 2: deformation continues for a long time (2–3 hours under the time scale in section 2.4) compared to how quickly the top layers reach maximal strain due to progressive consolidation of deeper sections as the fluid is gradually exuded. This effect is enhanced by the inhomogeneity of the aggrecan concentration, which effects a greater maximal deformation of the superficial zone and lesser maximal deformation of the deep zone than is seen when compared to a homogenised equivalent (Federico et al., 2009).

To understand the effect of boundary resistance, we first examine a static stress of non-dimensional magnitude $|\Sigma| = 15$. (Recall that this is equivalent to a load of 500 kPa using the parameters in table 1, as discussed in section 2.4.) Figure 3A depicts the evolution of true cartilage thickness $h(t) = 1 + \int_0^1 \varepsilon(z,t)\,dz$ for different values of Γ, calculated by numerical integration of eq. (3). For a free-flowing boundary (that is, $\Gamma = 0$) the classic displacement–time curve seen in confined compression tests with a free-flowing boundary is reproduced, with a basic consolidation time around 1–2 hours (Higginson et al., 1976; Mow et al., 1980). Increasing the boundary resistance clearly acts to slow down consolidation to some degree, but we would like to quantify this relationship.

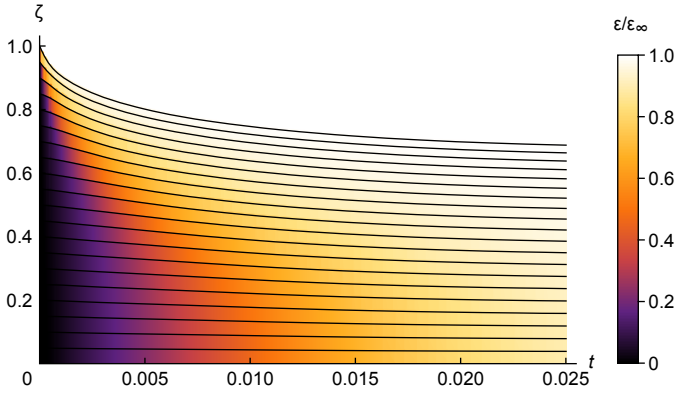

Figure 2: Consolidation under a static load; $|\Sigma| = 15$, $\Gamma = 0.05$. Lines are true material curves of initially equispaced points through the cartilage thickness, i.e. $\zeta(z,t) = z + \int_0^z \varepsilon(z',t)\,dz'$ against non-dimensional time t for constant values of z. Colour scheme indicates fraction of total eventual consolidation at each z through the thickness, i.e. $\varepsilon(z,t)/\lim_{t\to\infty}\varepsilon(z,t)$, showing the slower rate of consolidation near the bone than at the surface.

Free-boundary homogeneous consolidation obeys an exponential decay at large t (Verruijt, 1995), so we expect similar behaviour here. The effect of Γ can be seen in the global consolidation rate

$$\chi(t) = -\frac{d}{dt}\log(h(t) - h_\infty), \tag{8}$$

where h_∞ is the steady-state consolidated thickness as $t \to \infty$. (Recall that $p \to 0$ as $t \to \infty$ under a static stress, so h_∞ can be calculated by solving the steady-state stress balance $\Sigma = \sigma$ numerically for ε_∞ incrementally in z and then integrating.) The rate $\chi(t)$ is the instantaneous exponential decay constant, fitting $h(t) - h_\infty \propto e^{-\chi t}$ at a given t. Figure 3B indicates that our system does approach an exponential decay at large t: after a transient period of slower consolidation, χ approaches a constant. The rate of approach is slower for greater Γ and never faster than the free-boundary rate with $\Gamma = 0$. Indeed, we can use eqs. (3) and (4) to show that

$$\frac{dh}{dt} = \frac{p(1,t)}{\Gamma} = \frac{\sigma(1,t) - \Sigma}{\Gamma},$$

which clarifies the effect of Γ in retarding consolidation.

The precise impact of Γ on this long-term rate can be inferred by considering asymptotics of the system. For

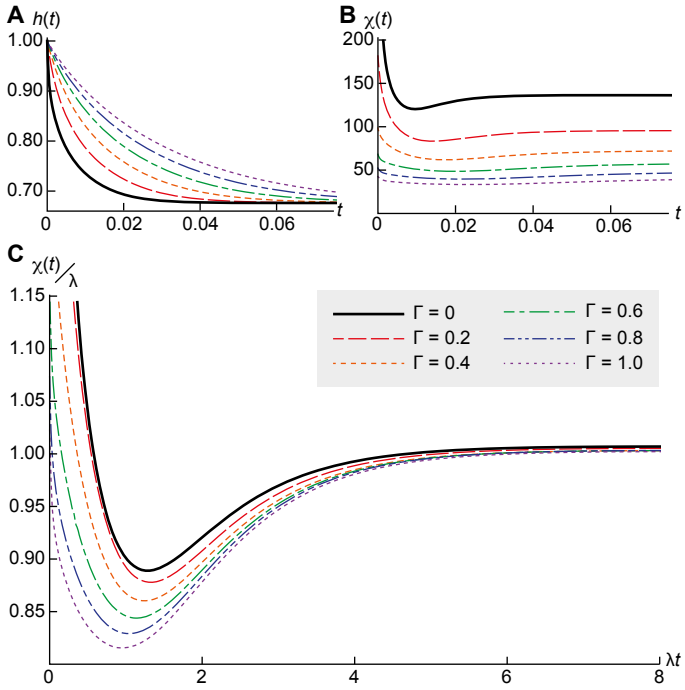

Figure 3: Consolidation under a static load of $|\Sigma| = 15$, for $\Gamma = 0$ (thick solid curve) and a uniform range between $\Gamma = 0.2$ and $\Gamma = 1$ (dashed curves). (A) Thickness $h(t)$ as a function of non-dimensional time t. Increasing Γ slows consolidation. (B) The consolidation rate $\chi(t)$. Higher Γ causes a later trough and slower long-term χ. (C) The rescaling $\chi(t)/\lambda$ against λt via the solution of eq. (12). Despite the non-uniform aggrecan concentration present in the simulations, the curves collapse remarkably well.

analytic tractability, we will suppose that the aggrecan concentration is uniform through the cartilage by replacing $c_0(z)$ with its spatial average $\overline{c_0}$; this renders the osmotic pressure Π and permeability k as functions purely of $\varepsilon(z)$, removing the direct dependence on z. Now, suppose we are at large t nearing the steady state $p = 0, \varepsilon = \varepsilon_\infty, \sigma = \Sigma$, where homogeneity implies that ε_∞ is also independent of z. Equilibrium $-p + \sigma = \Sigma$ implies

$$\frac{\partial p}{\partial z} = \frac{\partial \sigma}{\partial z} = \frac{\partial \sigma}{\partial \varepsilon}\frac{\partial \varepsilon}{\partial z}.$$

Recalling the effective permeability $K = k/(1+\varepsilon)$, eq. (3) then reads

$$\frac{\partial \varepsilon}{\partial t} = \frac{\partial}{\partial z}\left[K\frac{\partial \sigma}{\partial \varepsilon}\frac{\partial \varepsilon}{\partial z}\right]. \tag{9}$$

We will now expand about the $t \to \infty$ state. Let $K_\infty = K|_{\varepsilon=\varepsilon_\infty}$ and $\sigma_{\varepsilon,\infty} = [\partial\sigma/\partial\varepsilon]_{\varepsilon=\varepsilon_\infty}$. Assuming an exponential decay towards the steady state at leading order, write

$$\begin{aligned}\varepsilon &= \varepsilon_\infty + \eta\varepsilon_1(z)e^{-\lambda t} + O(\eta^2),\\ K &= K_\infty + O(\eta),\\ \frac{\partial\sigma}{\partial\varepsilon} &= \sigma_{\varepsilon,\infty} + O(\eta),\end{aligned}$$

where $\lambda > 0$ is the long-term consolidation rate and $\eta \ll 1$ is a small bookkeeping parameter. Substituting these into eq. (9) and discarding terms of $O(\eta^2)$ yields

$$-\lambda\varepsilon_1 = K_\infty\sigma_{\varepsilon,\infty}\frac{d^2\varepsilon_1}{dz^2}. \tag{10}$$

All that remains is to linearise the boundary conditions. Expanding σ about $\varepsilon = \varepsilon_\infty$ implies

$$p = \sigma - \Sigma = \eta\sigma_{\varepsilon,\infty}\varepsilon_1(z)e^{-\lambda t} + O(\eta^2). \tag{11}$$

Therefore, to first order in η, the bone boundary condition $p_z(0,t) = 0$ implies that $[d\varepsilon_1/dz]_{z=0} = 0$, and the surface boundary condition eq. (7) implies that $\varepsilon_1(1) = -\Gamma K_\infty[d\varepsilon_1/dz]_{z=1}$. We are therefore presented with an elementary Sturm–Liouville problem for the spectrum of decay rates λ.

Let $\nu^2 = \lambda/(K_\infty\sigma_{\varepsilon,\infty})$. (Note $\sigma_{\varepsilon,\infty} > 0$.) With the boundary conditions, eq. (10) has solution $\varepsilon_1(z) \propto \cos\nu z$ for ν satisfying

$$\cot\nu = \Gamma K_\infty\nu. \tag{12}$$

Properties of the function $\cot\nu$ guarantee that there always exists exactly one solution in $0 < \nu \leqslant \pi/2$ for all $\Gamma \geqslant 0$, which will be the dominant term. Equality is achieved precisely when $\Gamma = 0$, which yields the free-flow consolidation rate $\lambda = (\pi^2/4)K_\infty\sigma_{\varepsilon,\infty}$. Non-zero Γ moves ν away from $\pi/2$ towards 0, so the consolidation rate $\lambda \propto \nu^2$ falls. If Γ is still sufficiently small so that ν is close to $\pi/2$, then we can expand $\cot\nu \approx -(\nu - \pi/2)$ to get the approximations

$$\nu \approx \frac{\pi/2}{1+\Gamma K_\infty}, \qquad \lambda \approx \frac{(\pi/2)^2K_\infty\sigma_{\varepsilon,\infty}}{(1+\Gamma K_\infty)^2}.$$

At the other extreme when $\Gamma \gg 1$ and therefore $\nu \ll \pi/2$, we have $\cot \nu \approx 1/\nu$, giving the approximate solution

$$\nu \approx (\Gamma K_\infty)^{-1/2}, \qquad \lambda \approx \frac{\sigma_{\varepsilon,\infty}}{\Gamma}.$$

For intermediate values of Γ, neither approximation applies. In this case, eq. (12) has no exact analytic solution, but it is easy to solve numerically.

Figure 3C displays the rescaling of the consolidation curves $\chi(t)$ in fig. 3B by the solution λ of eq. (12) at the corresponding value of Γ; specifically, we plot $\lambda^{-1}\chi(t)$ against λt. Even though λ is based upon a spatially-averaged aggrecan distribution and is only a long-time rate, the curves cluster remarkably well: the rate minima have aligned, and all trend near to $\chi \to \lambda$. This analysis therefore gives us good approximations for the long term behaviour of consolidating cartilage as a function of Γ.

The analysis also supplies large-t approximations for the strain $\varepsilon(z,t)$ and, via eq. (11), the pressure $p(z,t)$, which both differ from their equilibrium values (ε_∞ and 0, respectively) in proportion to $e^{-\lambda t}\cos \nu z$. Thus an increased boundary resistance Γ actually has two effects: as well as increasing the time scale λ^{-1}, it also increases the spatial variation scale ν^{-1}. In other words, the resistance both slows down and smooths out the consolidation process.

4. Oscillatory loading

In the previous section, we investigated the effect of static loading on our cartilage model. However, everyday stress patterns are not static, but cyclic. Over time, if the pattern stays the same, the cartilage will approach a periodic state with the compression fluctuating about a long-term mean. Depending on the form and frequency of loading, the long-term mean may differ significantly from that obtained by applying the same average static load (Kääb et al., 1998). Characterising when and by how much these differences occur is important for understanding the limits of long-term cartilage homeostasis.

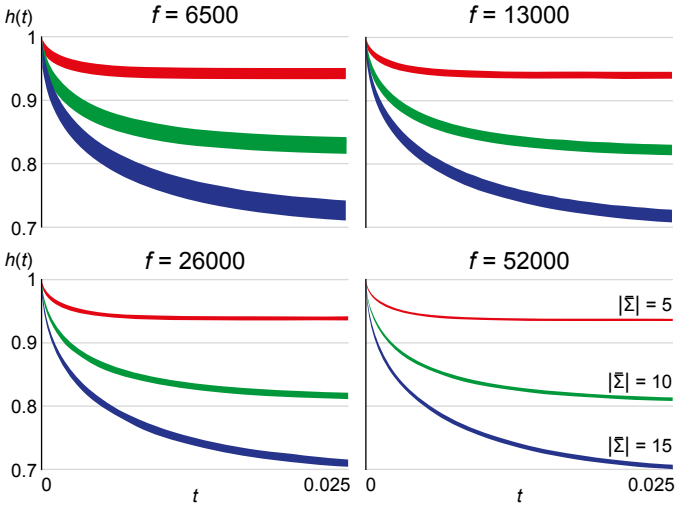

Figure 4: Envelope of variation of cartilage thickness $h(t)$ under oscillatory stress, with small boundary resistance $\Gamma = 0.01$, against non-dimensional time t. Four different non-dimensional frequencies f are shown, with the same three values of mean stress $\bar{\Sigma}$ (indicated) evaluated at each frequency. As f increases, the envelopes become progressively slimmer.

In this section, we will study the effect of oscillatory loading on our model. In particular, we will explore the effect of the boundary resistance Γ on strain and pressure variation, both globally and locally. We will see that even when the cartilage appears to be static globally, a region of persistent local strain oscillations remains in the superficial zone, whose magnitude and depth we can approximate.

4.1. Consolidation

We first demonstrate the oscillatory consolidation process by examining how the cartilage thickness $h(t)$ varies with load profile. Using a cyclic stress as in eq. (6) and setting $\Gamma = 0.01$, fig. 4 illustrates the envelope of $h(t)$ at varying frequency and mean stress, where the frequencies shown are equivalent to doubling from 1/64 Hz to 1/8 Hz under the time scale of section 2.4. Increasing the frequency damps the variation, suggesting that many real-world load patterns might be effectively simplified to some equivalent static load. We will return to this point later.

The value of Γ used above might seem rather small compared with the range we considered in the static con-

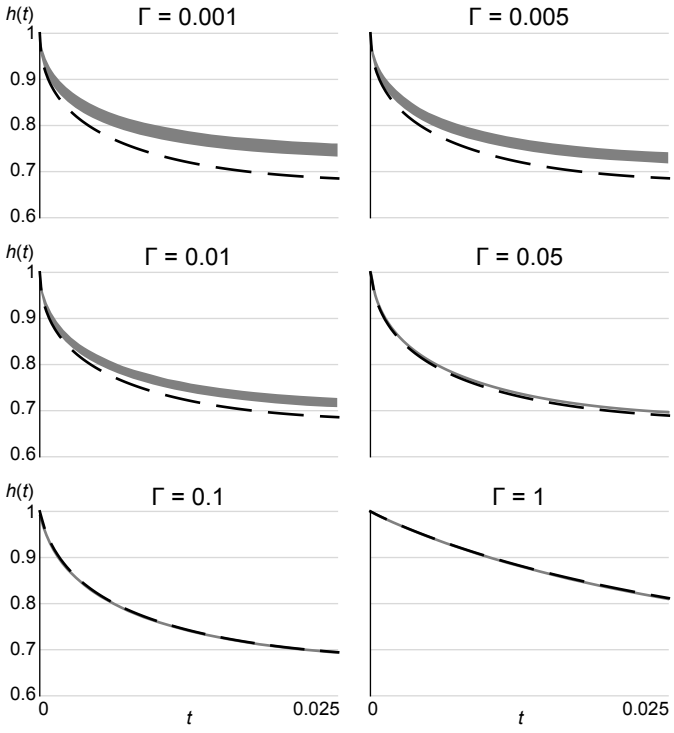

Figure 5: Cartilage thickness $h(t)$ under oscillatory ($f = 13000$; grey envelope of variation) versus static (dashed black) consolidation at $|\bar{\Sigma}| = 15$, for various indicated values of Γ, against non-dimensional time t. Greater Γ first brings oscillatory consolidation closer to that of static and narrows its envelope of variation, then slows down the long-term consolidation rate.

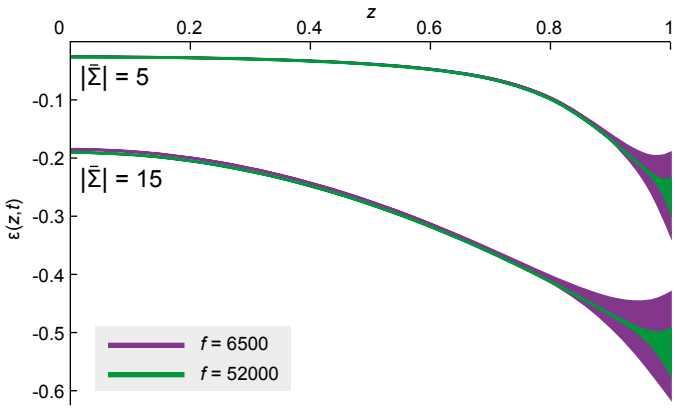

Figure 6: Envelope of variation of the local strain $\varepsilon(z,t)$ through the cartilage thickness z under oscillatory loading, after allowing time for consolidation, at moderate resistance $\Gamma = 0.1$. Two values of mean stress $\bar{\Sigma}$ are displayed, at two frequencies f each. The penetration depth of the strain variation corresponds in proportion to the superficial zone of cartilage. Variation is increased at higher stresses and decreased at higher frequencies.

solidation examples. In fact, small values of Γ markedly temper the variation in $h(t)$. Setting $|\bar{\Sigma}| = 15$ and $f = 13000$ (equivalent to 1/32 Hz), fig. 5 compares the envelope of $h(t)$ under oscillatory loading to that of static loading of the same mean stress at six values of Γ. As Γ increases to $\Gamma = 0.05$, cyclic variation in $h(t)$ is heavily suppressed and the envelope approaches the static loading curve. Thus even at this slow frequency, a small amount of boundary resistance lends temporal stability to the cartilage. Beyond $\Gamma = 0.05$, the behaviour enters the regime of fig. 3 where increasing resistance slows down the whole consolidation process.

However, there are important details missed by considering only the thickness $h(t)$. Figure 6 shows large-t envelopes of $\varepsilon(z,t)$ through the cartilage depth z for two values of mean stress at low and high frequency. There is a narrow but significant region near the surface where non-trivial cyclic deformation occurs, thinner for higher loading frequency; this effect has been seen in previous studies of cyclic loading (Suh et al., 1995), but is less pronounced here because of the moderating influence of the boundary resistance. Nevertheless, this behaviour means that we cannot neglect the effects of oscillations altogether when considering the local mechanical environment. As an aside, we note that the overlap of this region with the superficial zone of surface-parallel collagen and pancake-shaped chondrocytes seems unlikely to be coincidental (Wilson et al., 2006).

4.2. Superficial zone strain variation

We will now analytically quantify these superficial zone oscillations. By making some judicious approximations in the case of small oscillations, we can extract the parameter relationships governing the penetration depth, strain variability and compression wave propagation speed of the oscillating region.

Suppose we subject the cartilage to oscillatory loading $\Sigma(t)$ of period $\tau = 1/f$. Until specified otherwise, no particular form of $\Sigma(t)$ is assumed. For a periodic function F,

define the cycle mean

$$\langle F(t)\rangle = \frac{1}{\tau}\int_0^\tau F(t)\,dt.$$

For sufficiently large t, the strain $\varepsilon(z,t)$ is approximately periodic and decomposes into $\varepsilon(z,t) = \bar{\varepsilon}(z)+\delta(z,t)$, where $\bar{\varepsilon}(z) = \langle\varepsilon(z,t)\rangle$ and $\delta(z,t)$ has period τ with $\langle\delta(z,t)\rangle = 0$.

Now, suppose that the strain fluctuations are sufficiently small that we may use δ as an expansion parameter. This is the case for high frequency or low magnitude activity, or high boundary resistance. We view K and σ as functions of ε and z, rather than as functions of z and t, writing $K(\varepsilon;z)$ and $\sigma(\varepsilon;z)$. Linearising about $\bar{\varepsilon}$,

$$K(\varepsilon;z) = K(\bar{\varepsilon};z) + \delta(z,t)K_\varepsilon(\bar{\varepsilon};z),$$
$$\sigma(\varepsilon;z) = \sigma(\bar{\varepsilon};z) + \delta(z,t)\sigma_\varepsilon(\bar{\varepsilon};z).$$

Henceforth, subscripts F_ε refer to partial derivatives with respect to ε holding z constant, and Leibniz-style partial derivatives $\partial/\partial z$ (resp. $\partial/\partial t$) will denote holding t (resp. z) constant but *not* holding ε constant. In addition, where unspecified, the arguments of K, σ and derivatives are taken to be $(\bar{\varepsilon};z)$.

Similar linearisation of eq. (4) implies

$$\Sigma(t) = -p(z,t) + \sigma(\bar{\varepsilon};z) + \delta(z,t)\sigma_\varepsilon(\bar{\varepsilon};z). \qquad (13)$$

Linearising eq. (3) and substituting for p from eq. (13) gives

$$\frac{\partial\delta}{\partial t} = \frac{\partial}{\partial z}\left[K\frac{\partial\sigma}{\partial z} + K\frac{\partial}{\partial z}(\delta\sigma_\varepsilon) + \delta K_\varepsilon\frac{\partial\sigma}{\partial z}\right]. \qquad (14)$$

Since δ is periodic, we have $\langle\partial\delta/\partial t\rangle = 0$, so taking the cycle mean of eq. (14) and using $\langle\delta\rangle = 0$ gives

$$\frac{\partial}{\partial z}\left(K\frac{\partial\sigma}{\partial z}\right) = 0.$$

This shows $K\partial\sigma/\partial z$ is constant. The no-flow condition at $z = 0$ implies the constant is zero, so $\partial\sigma/\partial z \equiv 0$; in other words, $\sigma(\bar{\varepsilon},z)$ is constant in z.

Equation (14) now reads

$$\frac{\partial\delta}{\partial t} = \frac{\partial}{\partial z}\left[K\frac{\partial}{\partial z}(\delta\sigma_\varepsilon)\right]. \qquad (15)$$

At this stage we approximate K and σ_ε by their (presently unknown) values $K_1, \sigma_{\varepsilon,1}$ at $z = 1$ and neglect their z-derivatives, assuming that their variation with z is sufficiently small compared to their value over the superficial region of high δ-variation. Equation (15) then reduces to linear form

$$\frac{\partial\delta}{\partial t} = K_1\sigma_{\varepsilon,1}\frac{\partial^2\delta}{\partial z^2}, \qquad (16)$$

which is amenable to analytic solution. This diffusion equation immediately indicates that the depth of the oscillating region scales as $(K_1\sigma_{\varepsilon,1})^{1/2}$.

We solve eq. (16) by Fourier expansion in time. Decompose $\Sigma(t)$ and $\delta(z,t)$ as

$$\Sigma(t) = \bar{\Sigma} + \left(\sum_{n=1}^{\infty}\hat{\Sigma}_n e^{in\omega t} + \text{c.c.}\right),$$
$$\delta(z,t) = \sum_{n=1}^{\infty}\hat{\delta}_n(z)e^{in\omega t} + \text{c.c.},$$

where the angular frequency $\omega = 2\pi f = 2\pi/\tau$ and 'c.c.' denotes complex conjugate. Note that the Fourier coefficients $\hat{\Sigma}_n$ and $\hat{\delta}_n$ are, in general, complex. Taking the nth mode of eq. (16) implies

$$in\omega\hat{\delta}_n(z) = K_1\sigma_{\varepsilon,1}\frac{d^2\hat{\delta}(z)}{dz^2}.$$

This has solution $\hat{\delta}_n(z) = A_n e^{(1+i)\psi_n z} + B_n e^{-(1+i)\psi_n z}$, where we have defined the spatial growth and decay rates

$$\psi_n = \left(\frac{n\omega}{2K_1\sigma_{\varepsilon,1}}\right)^{1/2}.$$

Observe the complex exponents giving a temporal phase shift linear in z, indicating propagation of compression waves through the cartilage as opposed to instantaneous deformation. The term in B_n yields a mode with angular component $e^{i(n\omega t-\psi_n z)}$ which propagates in the direction of increasing z; this corresponds to a compression wave reflection off the bone at the base of the cartilage, whose minor contribution we neglect by setting $B_n = 0$.

We now use eq. (13) and the boundary condition at $z = 1$ to extract the coefficients A_n and cycle-averaged

strain $\bar{\varepsilon}$. Linearising eq. (7) in δ implies

$$p(1,t) \approx -\Gamma[K_1 + \delta(1,t)K_\varepsilon|_{z=1}] \left.\frac{\partial p}{\partial z}\right|_{z=1}$$
$$\approx -\Gamma K_1 \sigma_{\varepsilon,1} \left.\frac{\partial \delta}{\partial z}\right|_{z=1},$$

where we have used eq. (13) to substitute for p. Therefore, setting $z = 1$ in eq. (13) and recalling that σ is constant in z, we have

$$\Sigma(t) = \sigma + \left[\delta(1,t) + \Gamma K_1 \left.\frac{\partial \delta}{\partial z}\right|_{z=1}\right] \sigma_{\varepsilon,1}.$$

Taking the cycle mean yields $\bar{\Sigma} = \sigma$. This can be solved numerically for $\bar{\varepsilon}(z)$, which then enables calculation of K_1 and $\sigma_{\varepsilon,1}$. Taking higher modes, we have

$$\hat{\Sigma}_n = A_n e^{(1+i)\psi_n} \left[1 + \Gamma K_1 (1+i)\psi_n\right] \sigma_{\varepsilon,1},$$

which gives the coefficients A_n in terms of Σ_n.

This analysis finally gives us the strain oscillation

$$\delta(z,t) = \frac{1}{\sigma_{\varepsilon,1}} \sum_{n=1}^{\infty} \frac{\hat{\Sigma}_n e^{(z-1)\psi_n + i[(z-1)\psi_n + n\omega t]}}{1 + \Gamma K_1 (1+i)\psi_n} + \text{c.c.} \quad (17)$$

The magnitude of the surface deformations can be characterised by the $z = 1$ strain variance

$$\langle \delta(1,t)^2 \rangle = \frac{1}{\sigma_{\varepsilon,1}^2} \sum_{n=1}^{\infty} \frac{|\hat{\Sigma}_n|^2}{\left(\Gamma K_1 \psi_n + \frac{1}{2}\right)^2 + \frac{1}{4}}. \quad (18)$$

When $\Gamma = 0$, this is directly proportional to the variance of $\Sigma(t)$ and is independent of the oscillation frequency. A non-zero Γ has two effects: it decreases the amplitude of oscillations, with higher stress modes $\hat{\Sigma}_n$ subject to progressively stronger damping, and it introduces frequency dependence, with all modes subject to greater damping at higher frequencies (as seen in fig. 6).

Until this point, our derivation has not assumed any particular form of the stress $\Sigma(t)$. We now return to the 'semi-sine' stress function in eq. (6). The $n = 1$ mode of eq. (6) is $\hat{\Sigma}_1 = -i\pi\bar{\Sigma}/4$. Approximating eq. (18) by its first term and substituting for $\hat{\Sigma}_1$ gives a simplified expression for the standard deviation $\sqrt{\langle \delta(1,t)^2 \rangle} \approx \Delta$, where

$$\Delta = \frac{\pi|\bar{\Sigma}|}{4\sigma_{\varepsilon,1}} \left[\left(\Gamma K_1 \psi_1 + \frac{1}{2}\right)^2 + \frac{1}{4}\right]^{-1/2}. \quad (19)$$

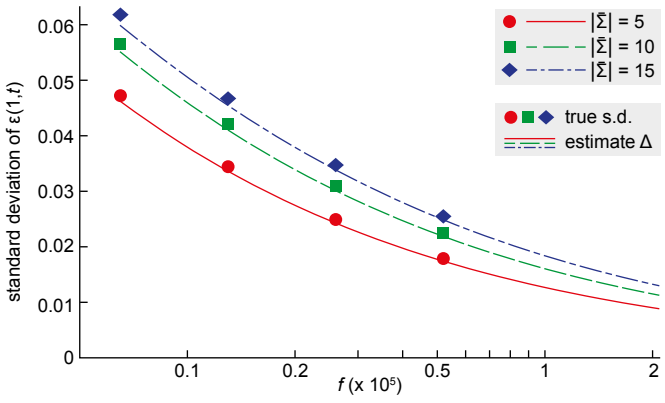

Figure 7: Approximate surface standard deviation Δ (lines) of eq. (19) compared to true standard deviation from numerical integration (symbols) as a function of loading frequency f (log scale), for three stress values $\bar{\Sigma}$ and at moderate resistance $\Gamma = 0.1$. Excellent agreement is seen, even at lower frequencies.

If $\Gamma = 0$, then Δ is independent of angular frequency ω. When $\Gamma > 0$, the high frequency limit reads

$$\Delta \approx \frac{\pi|\bar{\Sigma}|}{\Gamma} (8\sigma_{\varepsilon,1} K_1 \omega)^{-1/2}. \quad (20)$$

Figure 7 shows Δ as a function of frequency for three mean stresses compared with the true standard deviation $\sqrt{\text{Var}\,\varepsilon(1,t)}$ from a sample of numerical integrations of the full system, where $\Gamma = 0.1$. This value of Γ barely affects the static consolidation rate (see fig. 3), but does have a consolidated thickness close to that of the statically-loaded equivalent (see fig. 5) which lends accuracy to the approximation in eq. (19).

Each load cycle propagates as a compression wave through the cartilage. The $n = 1$ mode in eq. (17) has largest amplitude and therefore will dominate the propagation speed and the depth of the oscillating region; hence there is a wavespeed $v = \omega/\psi_1$ and a depth scale $d \sim 1/\psi_1$. As f (and so ω) increases, we see waves of decreasing magnitude $\Delta \sim \omega^{-1/2}$, with increasing propagation speed $v \sim \omega^{1/2}$ and decreasing propagation depth $d \sim \omega^{-1/2}$ over the propagation time $\tau \sim \omega^{-1}$. These compression waves can be visualised by plotting contours of constant $\varepsilon(z,t)$, as shown in fig. 8 for three different frequencies. The increase in propagation speed v manifests as shallower con-

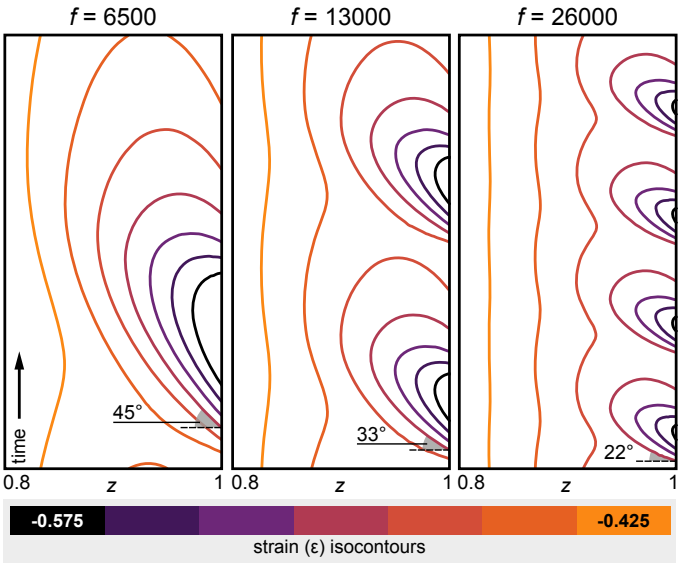

Figure 8: Contours of the local strain $\varepsilon(z,t)$ over non-dimensional time t within the superficial zone $0.8 < z < 1$ for three frequencies f, with mean stress $|\bar{\Sigma}| = 15$ and resistance $\Gamma = 0.1$. Timespan corresponds to one, two and four complete cycles for the frequencies from left to right. Contour levels are identical in each. Shallower lines (indicated) demonstrate faster compression waves, and shallower penetration of looping contours shows lessening depth of variation.

tour gradients, and the decrease in propagation depth d and magnitude Δ is seen in the shallower penetration of 'looping' contours.

The above analysis also yields the variation in fluid pressure. Using eq. (13) and approximating constants by their values at $z = 1$ as before, we find that

$$p(z,t) = \sum_{n=1}^{\infty} \hat{\Sigma}_n e^{in\omega t} \left[\frac{e^{(z-1)\psi_n + i(z-1)\psi_n}}{1 + \Gamma K_1 (1+i)\psi_n} - 1 \right] + \text{c.c.},$$

which gives the equivalent approximation to eq. (19) as

$$\sqrt{\langle p(1,t)^2 \rangle} \approx \frac{\pi |\bar{\Sigma}|}{\sqrt{2}} \left[\left(1 + \frac{1}{\Gamma K_1 \psi_1} \right)^2 + 1 \right]^{-1/2}.$$

When $\Gamma = 0$, this vanishes because a free-flowing boundary does not sustain any pressure. However, when $\Gamma > 0$ this approaches the constant $\pi|\bar{\Sigma}|/2$ in the high-frequency limit.

4.3. Equivalent stress

The solution above has captured the variations in oscillation amplitude, but it does not account for the change with frequency of the long-term average consolidated thickness $\bar{h} = \lim_{t' \to \infty} f \int_{t'}^{t'+1/f} h(t)\, dt$, clearly visible in fig. 4. At high frequency (and hence low Δ) $\bar{h}$ is close to that seen under the equivalent static stress, but lower frequencies deviate from this and consolidate to a lesser degree. We can find a simple estimate of this effect, at least within the superficial zone, by employing an extra term in the stress expansion.

As before, suppose that σ_ε, K and their ε-derivatives can be approximated in the superficial zone by their values at $z = 1$. Writing eq. (13) to the next order in δ and taking the cycle mean implies

$$\bar{\Sigma} \approx -\langle p \rangle + \sigma_1 + \tfrac{1}{2} \langle \delta^2 \rangle \sigma_{\varepsilon\varepsilon,1},$$

where we have used the second derivative $\sigma_{\varepsilon\varepsilon,1} = \sigma_{\varepsilon\varepsilon}|_{z=1}$. Requiring zero mean fluid flow at large t in tandem with the $z = 1$ boundary condition implies that, under our approximations, $\langle p \rangle = 0$. If we then use eq. (19) to estimate $\langle \delta^2 \rangle \approx \Delta^2$, we get

$$\bar{\Sigma} = \sigma_1 + \tfrac{1}{2} \Delta^2 \sigma_{\varepsilon\varepsilon,1}. \tag{21}$$

By substituting for the definitions of $\sigma_{\varepsilon\varepsilon,1}$ and Δ, this could be numerically solved for a more accurate $\bar{\varepsilon}$ than the first-order approximation $\bar{\Sigma} = \sigma_1$ we used before. The new strain will be smaller than the first-order approximation owing to the term in Δ^2. Alternatively, we can use this to define an equivalent stress Σ_{eq}: the static stress which would induce the same mean superficial strain $\bar{\varepsilon}$ as that of oscillatory consolidation of a specified frequency and mean stress $\bar{\Sigma}$. Static consolidation obeys $\Sigma_{\text{eq}} = \sigma_1$ as $t \to \infty$, so eq. (21) gives

$$\Sigma_{\text{eq}} = \bar{\Sigma} - \tfrac{1}{2} \Delta^2 \sigma_{\varepsilon\varepsilon,1}.$$

Note that $\sigma_{\varepsilon\varepsilon,1} < 0$, so $|\Sigma_{\text{eq}}| < |\bar{\Sigma}|$, and as $f \to \infty$ we have that $\Delta \to 0$ by eq. (20), so $\Sigma_{\text{eq}} \to \bar{\Sigma}$.

5. Discussion

Our results have important implications for the biomechanics of osteoarthritis development. In the introduction,

we discussed how chronic abnormal loading through behaviour or joint mechanics is a risk factor for OA. We will now explain how our results corroborate these risk factors and explain the onset of mechanically-induced OA.

A likely early stage in many forms of OA is when chondrocyte apoptosis overtakes chondrocyte proliferation. Two types of mechanical overload are known to cause apoptosis, namely excessive strain ε and excessive rate-of-strain $\partial\varepsilon/\partial t$ (Kurz et al., 2005), though more may exist. Assuming the transitory consolidation period has passed, these can be expressed in terms of the deep and superficial zones' mean strains $\bar{\varepsilon}_{\text{deep}}$ and $\bar{\varepsilon}_{\text{sup}}$, the superficial zone strain variation Δ and the loading frequency f. The first overload, excessive compressive strain, corresponds to $|\bar{\varepsilon}_{\text{deep}}|$ in the deep zone and $|\bar{\varepsilon}_{\text{sup}}| + \Delta$ in the superficial zone. The second overload, excessive rate-of-strain $\partial\varepsilon/\partial t$, will only occur in the superficial zone, where it corresponds to the product $f\Delta$. (If it were to occur in the deep zone, it would be the result of a traumatic instantaneous overload.) Considering how these change in different scenarios will indicate whether we expect to see mechanically-induced OA, and why.

Most striking are the consequences of a partial or total meniscectomy in the knee, known to be a high risk factor for OA (Papalia et al., 2011). Removal of the meniscus has two key effects: it increases the magnitude of the stress on the central cartilage region by decreasing the contact area, and it decreases the resistance to fluid efflux at the contact interface. In terms of our model parameters, $|\bar{\Sigma}|$ rises and Γ falls. This causes considerable growth of the oscillation variance Δ in eq. (20), as well as the more obvious rise in the mean strain magnitudes $|\bar{\varepsilon}_{\text{deep}}|$ and $|\bar{\varepsilon}_{\text{sup}}|$ through the rise in $|\bar{\Sigma}|$. Therefore, all the key overload gauges—$|\bar{\varepsilon}_{\text{deep}}|$, $|\bar{\varepsilon}_{\text{sup}}| + \Delta$ and $f\Delta$—will rise, causing increased apoptosis. A vicious cycle begins: a reduced cell density implies slower synthesis of aggrecan, which compromises the mechanical structure as the aggrecan content falls, leading to even greater overload and more apoptosis. As this cycle repeats unchecked, the tissue eventually degrades beyond useful function.

Even without as extreme a change as a meniscectomy, overloading can be induced merely by ligament injury or misalignment of the knee. In this case, though the flow resistance remains the same, the load distribution is altered and one side of the joint is subjected to a higher stress than is normal. Therefore, as for the meniscectomy, the stress magnitude $|\bar{\Sigma}|$ rises with potentially damaging results if the ligament weakness or joint misalignment is not corrected.

There is further potential for damage beyond overstraining. We saw that a decrease in the boundary resistance Γ will decrease the long-term consolidation time; in other words, the flux of fluid exiting the cartilage will start greater and decay faster than it did originally. This means that the fluid available for mixed mode lubrication between the joint faces will decrease quicker, increasing the duration of cartilage-on-cartilage contact and consequently degrading the superficial zone. The associated fibrillation of the collagen matrix in the superficial zone is another hallmark of early OA (Pritzker et al., 2006), potentially causing with a further fall in Γ because of the change in surface collagen geometry and density. Combining the consolidation time (section 3) with the equivalent static stress (section 4.3) provides a gauge of how quickly this high-friction regime will develop for different patterns of activity.

In fact, the equivalent stress gives us another way to classify activities by their potential for damage. It is possible that chondrocytes do not respond immediately to high strain, provided it is not extreme, but rather are only sensitive to the average strain over many cycles (Chen et al., 2003). The equivalent stress provides a means to quickly classify which patterns of daily activity are likely to be dangerous in this way and which are not. In particular, by this measure, low-frequency activities will be less destructive than high-frequency activities of the same aver-

age stress.

To model the maintenance or loss of cartilage integrity over the course of years of activity, we must be able to efficiently describe the consequences of any short- or long-term change in the biomechanical parameters. The derivations we have presented here provide exactly this. In the future, we hope to couple such a biomechanical model with lifestyle and genetic data to enable effective intervention through early prediction of osteoarthritis.

Acknowledgement

This research was funded by NHMRC Project Grant 1051538.

Appendix: Strain equation

To derive the dynamics of the material response to stress, we follow Gibson et al. (1967, 1981) and McNabb (1960). Let ζ be the Eulerian ('laboratory frame') position coordinate, with the bone surface at $\zeta = 0$ and the cartilage extending up to $\zeta = h(t)$ as the stresses and deformations vary over time t. Now, let z be the Lagrangian ('cartilage frame') coordinate, where the cartilage always extends between $z = 0$ and $z = H$. We can regard one of these coordinate systems as a function of the other; thus, at some time t, a slice of cartilage at z will be at a position $\zeta(z,t)$ in the laboratory frame. In particular, the total consolidated depth is $h(t) = \zeta(H,t)$, and the steady unloaded configuration is $\zeta(z,0) = z$.

Let $n(z,t)$ be the porosity field, i.e. the proportion of liquid to solid phase. Consider a small material element between z and $z+\delta z$ at $t = 0$. The solid phase has mass $\rho[1-n(z,0)]\delta z$, where ρ is the solid phase density. At some future time t, the element lies between $\zeta(z,t)$ and $\zeta(z+\delta z,t)$ with new thickness $\delta\zeta = \zeta(z+\delta z,t) - \zeta(z,t) = (\partial\zeta/\partial z)\delta z$, and has solid phase mass $\rho[1-n(z,t)]\delta\zeta$ by incompressibility. Conservation of solid mass therefore reads

$$1 - n(z,0) = [1 - n(z,t)]\frac{\partial \zeta}{\partial z}. \tag{A.1}$$

Let the velocities of the solid and fluid phases be v_s and v_f, respectively. Fluid mass balance within a Lagrangian unit volume plus fluid incompressibility implies

$$\frac{\partial q}{\partial z} + \frac{\partial}{\partial t}\left(n\frac{\partial \zeta}{\partial z}\right) = 0, \tag{A.2}$$

where we define the specific discharge $q = n(v_f - v_s)$.

The net flux q is taken to obey Darcy's law, wherein the pressure gradient must be referred to the Eulerian frame, not the Lagrangian. Thus q obeys

$$q = -k\frac{\partial p}{\partial \zeta},$$

which implies

$$q\frac{\partial \zeta}{\partial z} = -k\frac{\partial p}{\partial z}$$

after changing variable. Substituting this into the fluid mass balance eq. (A.2) gives

$$\frac{\partial}{\partial z}\left(-k\frac{\partial p}{\partial z}\Big/\frac{\partial \zeta}{\partial z}\right) + \frac{\partial}{\partial t}\left(n\frac{\partial \zeta}{\partial z}\right) = 0. \tag{A.3}$$

At this stage we depart from Gibson et al. (1967, 1981) and replace the porosity n with volume strain ε to obtain a more 'traditional' poroelasticity equation (McNabb, 1960; Verruijt, 1995). Let

$$\varepsilon = \frac{\delta\zeta - \delta z}{\delta z} = \frac{\partial \zeta}{\partial z} - 1 = \frac{1 - n(z,0)}{1-n} - 1,$$

where the final equality is implied by solid mass balance eq. (A.1). Then the porosity n reads

$$n = 1 - \frac{1-n(z,0)}{1+\varepsilon} = \frac{\varepsilon + n(z,0)}{1+\varepsilon}.$$

Substituting this into eq. (A.3) gives the final equation

$$\frac{\partial \varepsilon}{\partial t} = \frac{\partial}{\partial z}\left(\frac{k}{1+\varepsilon}\frac{\partial p}{\partial z}\right)$$

as quoted by McNabb (1960). Note that the initial porosity $n(z,0)$ is now rendered entirely implicit, and would only be required to compute the fluid discharge velocity $v_f - v_s$ as opposed to the flux q. Note also that this is identical to what would be obtained through an infinitesimal strain theory approach, except that the permeability k has been adjusted to an effective permeability $K = k/(1+\varepsilon)$ accounting for the volume change.

References

Ateshian, G. A., 2009. The role of interstitial fluid pressurization in articular cartilage lubrication. J. Biomech. 42 (9), 1163–1176.

Ateshian, G. A., Warden, W. H., Kim, J. J., Grelsamer, R. P., Mow, V. C., 1997. Finite deformation biphasic material properties of bovine articular cartilage from confined compression experiments. J. Biomech. 30 (11), 1157–1164.

Bader, D. L., Salter, D. M., Chowdhury, T. T., 2011. Biomechanical influence of cartilage homeostasis in health and disease. Arthritis 2011.

Batchelor, G. K., 2000. An introduction to fluid dynamics. Cambridge University Press.

Bathe, M., Rutledge, G. C., Grodzinsky, A. J., Tidor, B., 2005. Osmotic pressure of aqueous chondroitin sulfate solution: a molecular modeling investigation. Biophys. J. 89 (4), 2357–2371.

Biot, M. A., 1955. Theory of elasticity and consolidation for a porous anisotropic solid. J. Appl. Phys. 26 (2), 182–185.

Bitton, R., 2009. The economic burden of osteoarthritis. Am. J. Manag. Care 15 (8), S230.

Carter, D. R., Wong, M., 2003. Modelling cartilage mechanobiology. Philos. T. R. Soc. Lon. B 358 (1437), 1461–1471.

Changoor, A., Nelea, M., Méthot, S., Tran-Khanh, N., Chevrier, A., Restrepo, A., Shive, M. S., Hoemann, C. D., Buschmann, M. D., 2011. Structural characteristics of the collagen network in human normal, degraded and repair articular cartilages observed in polarized light and scanning electron microscopies. Osteoarthr. Cartilage 19 (12), 1458–1468.

Chen, A. C., Bae, W. C., Schinagl, R. M., Sah, R. L., 2001. Depth- and strain-dependent mechanical and electromechanical properties of full-thickness bovine articular cartilage in confined compression. J. Biomech. 34 (1), 1–12.

Chen, C.-T., Bhargava, M., Lin, P. M., Torzilli, P. A., 2003. Time, stress, and location dependent chondrocyte death and collagen damage in cyclically loaded articular cartilage. J. Orthop. Res. 21 (5), 888–898.

Coggon, D., Croft, P., Kellingray, S., Barrett, D., McLaren, M., Cooper, C., 2000. Occupational physical activities and osteoarthritis of the knee. Arthritis Rheum. 43 (7), 1443–1449.

Comper, W. D., 1991. Physicochemical aspects of cartilage extracellular matrix. In: Cartilage: Molecular Aspects. Taylor & Francis, London, pp. 59–96.

Comper, W. D., Lyons, K. C., 1993. Non-electrostatic factors govern the hydrodynamic properties of articular cartilage proteoglycan. Biochem. J. 289, 543–547.

Federico, S., Grillo, A., Giaquinta, G., Herzog, W., 2009. A semi-analytical solution for the confined compression of hydrated soft tissue. Meccanica 44 (2), 197–205.

Gibson, R. E., England, G. L., Hussey, M. J. L., 1967. The theory of one-dimensional consolidation of saturated clays. I. Finite non-linear consolidation of thin homogeneous layers. Géotechnique 17 (3), 261–273.

Gibson, R. E., Schiffman, R. L., Cargill, K. W., 1981. The theory of one-dimensional consolidation of saturated clays. II. Finite non-linear consolidation of thick homogeneous layers. Can. Geotech. J. 18 (2), 280–293.

Gleghorn, J. P., Bonassar, L. J., 2008. Lubrication mode analysis of articular cartilage using Stribeck surfaces. J. Biomech. 41 (9), 1910–1918.

Goggs, R., Carter, S. D., Schulze-Tanzil, G., Shakibaei, M., Mobasheri, A., 2003. Apoptosis and the loss of chondrocyte survival signals contribute to articular cartilage degradation in osteoarthritis. Vet. J. 166 (2), 140–158.

Goldring, M. B., Marcu, K. B., 2009. Cartilage homeostasis in health and rheumatic diseases. Arthritis Res. Ther. 11 (3), 224.

Grodzinsky, A. J., Levenston, M. E., Jin, M., Frank, E. H., 2000. Cartilage tissue remodeling in response to mechanical forces. Annu. Rev. Biomed. Eng. 2 (1), 691–713.

Haemer, J. M., Carter, D. R., Giori, N. J., 2012. The low permeability of healthy meniscus and labrum limit articular cartilage consolidation and maintain fluid load support in the knee and hip. J. Biomech. 45 (8), 1450–1456.

Halonen, K. S., Mononen, M. E., Jurvelin, J. S., Töyräs, J., Salo, J., Korhonen, R. K., 2014. Deformation of articular cartilage during static loading of a knee joint—Experimental and finite element analysis. J. Biomech. 47 (10), 2467–2474.

Han, E., Chen, S. S., Klisch, S. M., Sah, R. L., 2011. Contribution of proteoglycan osmotic swelling pressure to the compressive properties of articular cartilage. Biophys. J. 101 (4), 916–924.

Higginson, G. R., Litchfield, M. R., Snaith, J., 1976. Load–displacement–time characteristics of articular cartilage. Int. J. Mech. Sci. 18 (9), 481–486.

Hodge, W. A., Fijan, R. S., Carlson, K. L., Burgess, R. G., Harris, W. H., Mann, R. W., 1986. Contact pressures in the human hip joint measured in vivo. Proc. Natl. Acad. Sci. U.S.A. 83 (9), 2879–2883.

Hunziker, E. B., 2002. Articular cartilage repair: basic science and clinical progress. A review of the current status and prospects. Osteoarthr. Cartilage 10 (6), 432–463.

Hunziker, E. B., Quinn, T. M., Häuselmann, H.-J., 2002. Quantitative structural organization of normal adult human articular cartilage. Osteoarthr. Cartilage 10 (7), 564–572.

Jadin, K. D., Wong, B. L., Bae, W. C., Li, K. W., Williamson, A. K., Schumacher, B. L., Price, J. H., Sah, R. L., 2005. Depth-varying density and organization of chondrocytes in immature and mature bovine articular cartilage assessed by 3D imaging and analysis. J.

Histochem. Cytochem. 53 (9), 1109–1119.

Jones, A. R., Chen, S., Chai, D. H., Stevens, A. L., Gleghorn, J. P., Bonassar, L. J., Grodzinsky, A. J., Flannery, C. R., 2009. Modulation of lubricin biosynthesis and tissue surface properties following cartilage mechanical injury. Arthritis Rheum. 60 (1), 133–142.

Kääb, M. J., Ito, K., Clark, J. M., Nötzli, H. P., 1998. Deformation of articular cartilage collagen structure under static and cyclic loading. J. Orthop. Res. 16 (6), 743–751.

Katta, J., Jin, Z., Ingham, E., Fisher, J., 2008. Biotribology of articular cartilage—a review of the recent advances. Med. Eng. Phys. 30 (10), 1349–1363.

Kiani, C., Chen, L., Wu, Y. J., Yee, A. J., Yang, B. B., 2002. Structure and function of aggrecan. Cell Res. 12 (1), 19–32.

Klein, T. J., Chaudhry, M., Bae, W. C., Sah, R. L., 2007. Depth-dependent biomechanical and biochemical properties of fetal, newborn, and tissue-engineered articular cartilage. J. Biomech. 40 (1), 182–190.

Korhonen, R. K., Laasanen, M. S., Töyräs, J., Rieppo, J., Hirvonen, J., Helminen, H. J., Jurvelin, J. S., 2002. Comparison of the equilibrium response of articular cartilage in unconfined compression, confined compression and indentation. J. Biomech. 35 (7), 903–909.

Kurz, B., Lemke, A. K., Fay, J., Pufe, T., Grodzinsky, A. J., Schünke, M., 2005. Pathomechanisms of cartilage destruction by mechanical injury. Ann. Anat. 187 (5), 473–485.

Maroudas, A., 1976. Balance between swelling pressure and collagen tension in normal and degenerate cartilage. Nature 260 (5554), 808–809.

McCutchen, C. W., 1962. The frictional properties of animal joints. Wear 5 (1), 1–17.

McNabb, A., 1960. A mathematical treatment of one-dimensional soil consolidation. Q. Appl. Math. 17 (4), 337–347.

Mononen, M. E., Mikkola, M. T., Julkunen, P., Ojala, R., Nieminen, M. T., Jurvelin, J. S., Korhonen, R. K., 2012. Effect of superficial collagen patterns and fibrillation of femoral articular cartilage on knee joint mechanics—A 3D finite element analysis. J. Biomech. 45 (3), 579–587.

Mow, V. C., Holmes, M. H., Michael Lai, W., 1984. Fluid transport and mechanical properties of articular cartilage: a review. J. Biomech. 17 (5), 377–394.

Mow, V. C., Kuei, S. C., Lai, W. M., Armstrong, C. G., 1980. Biphasic creep and stress relaxation of articular cartilage in compression: theory and experiments. J. Biomech. Eng. 102 (1), 73–84.

Muir, H., Bullough, P., Maroudas, A., 1970. The distribution of collagen in human articular cartilage with some of its physiological implications. J. Bone Joint Surg. Br. 52 (3), 554–563.

Newman, A. P., 1998. Articular cartilage repair. Am. J. Sport. Med. 26 (2), 309–324.

Nieminen, M. T., Rieppo, J., Töyräs, J., Hakumäki, J. M., Silvennoinen, J., Hyttinen, M. M., Helminen, H. J., Jurvelin, J. S., 2001. T2 relaxation reveals spatial collagen architecture in articular cartilage: a comparative quantitative mri and polarized light microscopic study. Magn. Reson. Med. 46 (3), 487–493.

Papalia, R., Del Buono, A., Osti, L., Denaro, V., Maffulli, N., 2011. Meniscectomy as a risk factor for knee osteoarthritis: a systematic review. Brit. Med. Bull. 99 (1), 89–106.

Pierce, D. M., Ricken, T., Holzapfel, G. A., 2013. A hyperelastic biphasic fibre-reinforced model of articular cartilage considering distributed collagen fibre orientations: continuum basis, computational aspects and applications. Comput. Method. Biomec. 16 (12), 1344–1361.

Pritzker, K. P. H., Gay, S., Jimenez, S. A., Ostergaard, K., Pelletier, J.-P., Revell, P. A., Salter, D. v. d., Van den Berg, W. B., 2006. Osteoarthritis cartilage histopathology: grading and staging. Osteoarthr. Cartilage 14 (1), 13–29.

Sandell, L. J., Aigner, T., 2001. Articular cartilage and changes in arthritis. An introduction: cell biology of osteoarthritis. Arthritis Res. 3 (2), 107–113.

Schinagl, R. M., Ting, M. K., Price, J. H., Sah, R. L., 1996. Video microscopy to quantitate the inhomogeneous equilibrium strain within articular cartilage during confined compression. Ann. Biomed. Eng. 24 (4), 500–512.

Shepherd, D. E. T., Seedhom, B. B., 1999. Thickness of human articular cartilage in joints of the lower limb. Ann. Rheum. Dis. 58 (1), 27–34.

Smith, D. W., Gardiner, B. S., Davidson, J. B., Grodzinsky, A. J., 2013. Computational model for the analysis of cartilage and cartilage tissue constructs. J. Tissue Eng. Regen. M.

Suh, J.-K., Li, Z., Woo, S. L. Y., 1995. Dynamic behavior of a biphasic cartilage model under cyclic compressive loading. J. Biomech. 28 (4), 357–364.

Tepic, S., Macirowski, T., Mann, R. W., 1983. Mechanical properties of articular cartilage elucidated by osmotic loading and ultrasound. Proc. Natl. Acad. Sci. U.S.A. 80 (11), 3331–3333.

Verruijt, A., 1995. Computational geomechanics. Vol. 7. Springer.

Wedig, M. L., Bae, W. C., Temple, M. M., Sah, R. L., Gray, M. L., 2005. [GAG] profiles in "normal" human articular cartilage. In: Proceedings of the 51st Annual Meeting of the Orthopaedic Research Society. p. 0358.

Wilson, W., Driessen, N. J. B., van Donkelaar, C. C., Ito, K., 2006. Prediction of collagen orientation in articular cartilage by a collagen remodeling algorithm. Osteoarthr. Cartilage 14 (11), 1196–1202.

Wilson, W., Huyghe, J. M., van Donkelaar, C. C., 2007. Depth-dependent compressive equilibrium properties of articular cartilage explained by its composition. Biomech. Model. Mechan. 6 (1-

2), 43–53.

Wong, M., Carter, D. R., 2003. Articular cartilage functional histomorphology and mechanobiology: a research perspective. Bone 33 (1), 1–13.

Zhang, L., Miramini, S., Smith, D. W., Gardiner, B. S., Grodzinsky, A. J., 2014. Time evolution of deformation in a human cartilage under cyclic loading. Ann. Biomed. Eng., to appear.